Measurement 187 (2022) 110361

Contents lists available at ScienceDirect

Measurement

journal homepage: www.elsevier.com/locate/measurement

Steel type determination by spark test image processing with machine learning

Pedro José Pacheco Kerscher [a], Jean Schmith [a,*], Eduardo Augusto Martins [a,b], Rodrigo Marques de Figueiredo [a], Armando Leopoldo Keller [a]

[a] Escola Politécnica, Universidade do Vale do Rio dos Sinos - Unisinos. Av. Unisinos, 950, CEP 93022-00, São Leopoldo, Brazil
[b] ittFuse Institute, Universidade do Vale do Rio dos Sinos - Unisinos. Av. Unisinos, 950, CEP 93022-00, São Leopoldo, Brazil

ARTICLE INFO

Keywords:
Steel type determination
Spark testing
Steel carbon content
Image processing
Machine learning

ABSTRACT

The spark test method is a simple and low-cost method in which an operator with special skills observes the sparks emitted by a grinding wheel in contact with the steel in order to identify the material of the sample. However, the operator might classify erroneously two different steel materials with close spark characteristics. Therefore, we propose a method that extracts features from images captured from the spark test method and uses these features as input on machine learning models. The regression models predicted the carbon content of steel with 8% error while the classifiers had 82% of accuracy. The classifiers models had good results with few confusion points and regression models had low error. Regarding the confusion points, the regression algorithms could solve the misclassification by predicting the carbon content of the sample and increasing accuracy. The proposed method is suitable for real-time and shop floor applications.

1. Introduction

The industry becomes more autonomous every day. This evolution demands more automatic and smart systems, making the industry even more efficient. In the same direction, the industry quality control and process analysis must increase the attention to raw material. One of the most important raw materials in industry is steel and, therefore, its accurate determination in production lines is of prime importance. The most common technique for characterizing steel materials is the microstructural analysis, through optical or scanning electron microscopy. There are also additional methods such as chemical composition analysis, x-ray diffraction and microanalysis. However, these traditional classification methods demand sample preparation, which is time-consuming.

Previously, several works presented methods to make steel classification in laboratory more effective. Magallanes et al. [1] classified steel with chemical composition features and artificial neural networks. Mohamad et al. [2] studied the fracture characteristics with fuzzy C-means clustering. Dobrzanski et al. [3] studied the internal damage through the analysis of the metallographic images obtained in the scanning electron microscope. Segreto et al. [4] used the cutting force measurement and principal component analysis for the chip form classification in carbon steel. Dobrzanski et al. [5] studied the hardenability as a feature to determine steel classifications with neural networks. The microstructures are also common features used to classify steels with deep learning methods [6,7]. Xu et al. [8] classified the surface defects using multi-scale features. Surface defect classifications are also studied with convolutional neural networks [9–12]. Defect recognition in additive manufacturing, also using convolutional neural networks, was proposed by Caggiano et al. [13]. Laser spectroscopy with support vector machines and random forest was reported as a method for steel materials classification [14,15]. The use of non-destructive shock indentation test and artificial neural networks was proposed by Beskopylny et al. [16] for steel grades classification.

Although many methods reported in the literature for classifying steels in laboratory have real-time results, the preparation of samples can take some time. Furthermore, these methods are not applicable to the shop floor. Thus, many industries prefer to use the traditional spark test.

The use of the spark testing method started around 1909 and it is widely used nowadays for being a fast, easy to implement and low-cost method. This method consists on observing the sparks emitted by a grinding wheel in contact with steel material. The formation of sparks generated through the contact between the grinder and the steel occurs due to a reaction between oxygen and carbon. As the grinder detaches the small particles from the steel, the contact and friction

* Corresponding author.
E-mail addresses: pedrokerscher@outlook.com (P.J.P. Kerscher), jschmith@unisinos.br (J. Schmith), eamartins@unisinos.br (E.A. Martins), marquesf@unisinos.br (R.M.d. Figueiredo), alkeller@unisinos.br (A.L. Keller).

https://doi.org/10.1016/j.measurement.2021.110361
Received 16 September 2021; Accepted 17 October 2021
Available online 9 November 2021

between the two materials increases the temperature that can also rise by an instantaneous combustion. This effect is the result of the rapid oxidation of the surface of small particles that are pulled out of the steel sample. The steel particles are heated and fuse with each other, at least superficially, and tend to become spherical. Oxygen and carbon react in the heated particles and produce carbon dioxide. The scale of oxides formed on a simple carbon steel is not very tenacious and easily detaches. The gas that forms inside the heated sphere escapes through the fractured surface and gives rise to sparks [17].

Despite its popularity, the spark test method requires an operator with special skills and expertise for the spark pattern recognition [18]. The operator may make mistakes on steel material classification. Therefore, automated methods based on image processing and machine learning became an interesting solution for more accurate classifications of steel materials.

Previous works reported image processing methods to determine the carbon content on steel materials using the spark test method. Takeo Takata [19] developed a method to measure carbon content using image processing from the characteristics of sparks. This method detected the explosion sparks and the streamline sparks from the images. Next, the spark rate was calculated by dividing the number of explosion sparks by the number of all sparks. The accuracy reported was about ±0.05%. However, the proposed counting method of explosion sparks is difficult to implement accurately. In another work, the spark observation of fourteen different grades of steel using spark testing and image processing was conducted by Dalke et al. [18]. They studied the behavior of the sparks compared to a fixed inch scale drawn at the black background of the image. A reference manual with the experiments was created for academic purposes. Recently, Deng et al. [20] used the images of spark testing and showed that the fractal dimension of sparks has a good correlation with carbon content. They plotted the carbon content against fractal dimension and fitted by an natural logarithm function using the least squares method. The carbon measurement error was about 0.06%. Despite the existence of works with image processing and spark testing, none proposes to classify materials automatically using machine learning.

Therefore, the aim of this work is to present an automatic method for classification and carbon content estimation of steel. The method is suitable for real time applications and applicable to industries production lines. The proposed method extracts a set of features from spark testing images and uses it as input into machine learning models to determine the steel material.

2. Materials and methods

The proposed method for steel carbon content estimation and classification is based on the video capture from the spark test method. Fig. 1 illustrates the block diagram of the proposed method. To ensure that the videos of all samples have the same setup, we developed a device for fixing the grinding machine and the sample. After the video was captured, the image processing step convert the video into image sequences (e.g. each frame of the video is an image). All the images are then converted into grayscale images and the sparks are segmented. Finally, the features of each steel sample are extracted from the images.

The regression algorithms are machine learning models suitable for the carbon percentage estimation of steel samples. We tested several regression models, and two of them estimated the percentage of carbon with low error: Random Forest Regression (RFR) and Support Vector Regression (SVR).

Along with the regression models, it was also interesting to classify the steel among all selected materials. Image classification can be effectively performed by Convolutional Neural Networks (CNN). However, CNNs demands high computing capacity and memory space. The choice for the activation function may be very challenging as well, and finally finding a set of weights to best map the problem by iterative solutions can take days of computer processing and be memory consuming. Thus,

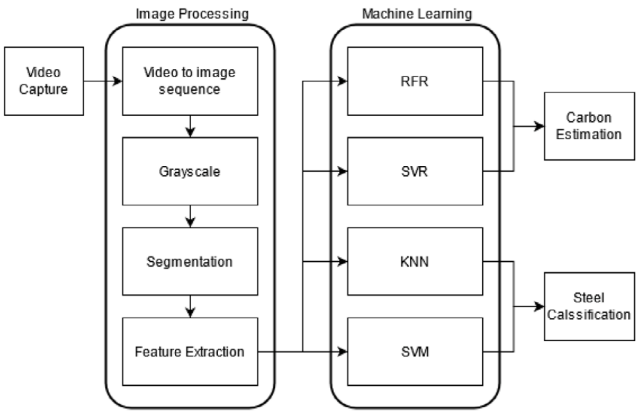

Fig. 1. Diagram of the proposed method for carbon content estimation and steel classification.

for faster results with lower computing capacity, machine learning classifier models were used. We tested some models and two had the best accuracy in steel classification: Support Vector Machine (SVM) and K-Nearest Neighbors (KNN).

The features extracted from the images were standardized and the same dataset was used in all machine learning models. The analysis of the results from machine learning models showed that the two approaches, regression and classification, must be evaluated together to determine the steel material.

The method was developed using OpenCV library [21] for the image processing, scikit-learn library [22] for the machine learning applications and Python programming. All steps of the method are detailed in the following sections.

2.1. Video capture setup

The spark testing method is based on the observation of sparks emitted from the contact of a grinding wheel with the steel material. Needless to say, the force applied to the grinding wheel may change the behavior of sparks [17]. To minimize the force variation effect, we developed a device for fixing the steel sample, and the grinding machine is fixed on a seesaw, shown in Fig. 2. The force applied to the material is proportional to the weight of the grinding machine and is easily determined. In our setup the computed force applied resulted in $F = 23$ N. We used the grinding machine ™Black+Decker G720 with disks for steel from ™Bosch of 115 mm diameter and 2.5 mm thickness. The device was fixed on a structure 0.8 m from the floor.

We did several camera positions experiments, with the best results being in front of the grinding machine. Therefore, the camera was positioned in front of the developed device on a tripod. The distance between the device and the camera was 1.17 m. The distance of the camera from the floor was 0.6 m. We used the camera Canon™EOS Rebel T4i. The complete setup is shown in Fig. 3.

For better separation of sparks from the background, the videos were recorded in a dark room. The camera focus was manually adjusted to avoid differences between videos. Each frame of video was converted into an image. The videos are 3 to 7 s long and the recording camera resolution is 96 dpi (dots per inch) with 30 fps (frames per second). The videos were then converted into an ensemble of images of 1920 × 1080 pixels. From these images we studied 5 different features of sparks behavior: image entropy, interquartile of sparks area distribution, the median of spark area distribution, the quantity of sparks and the sum of sparks areas.

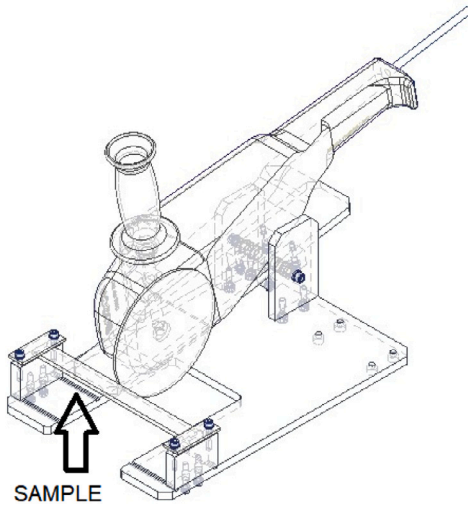

Fig. 2. Device for fixing the sample. The grinding machine was fixed to the seesaw.

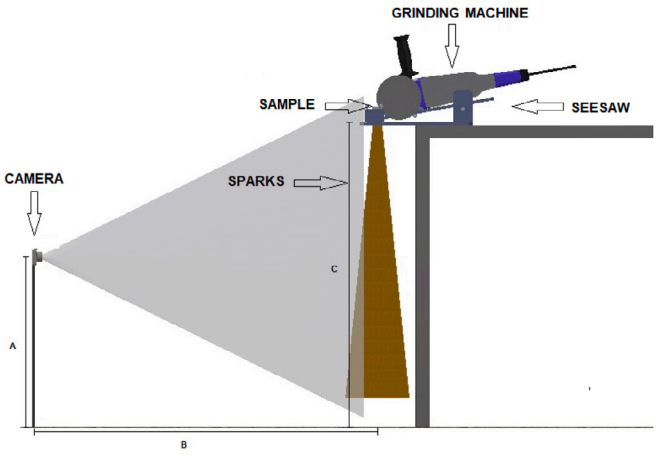

Fig. 3. Measurement setup. The distances indicated in the figure are $A = 0.6$ m, $B = 1.17$ m and $C = 0.8$ m.

2.2. Steel samples

The SAE (Society of Automotive Engineers) classification uses a logic that allows knowing carbon content of steel simply by knowing the values of the last two digits. The first two digits of this designation identify the main alloy elements present in steel, given in percentage by weight. We chose three steel samples of SAE classification, SAE1020, SAE1045 and SAE5160, which have a nominal carbon content of 0.20%, 0.45% and 0.60% respectively. The SAE1020 and SAE1045 are designated as carbon steels and the SAE5160 has 1% of chromium.

Further, we chose six tool steels: H13, P20, S1, O1, D2 and D6. The H13 have high content of chromium, tungsten, molybdenum and vanadium in addition to carbon. The P20 steel contains carbon, nickel and chromium as its main alloying elements. The composition of S1 contains carbon, manganese, silicon, chromium, tungsten and molybdenum. O1 steel has manganese, chromium, tungsten and carbon in its composition. The D2 and D6 are high carbon and high chromium tempered steels.

The chosen materials are listed in Table 1 with carbon range from 0.205% to 2.125%. It is important to note that the carbon content varies due to the production process, thus, instead of the nominal values, we considered the mean of that variation as the target for the machine learning models. The carbon variation of the samples was provided by the supplier [23]. Examples of spark test images from each material are presented in Fig. 4.

Table 1
List of sample steel materials with the carbon content variation provided by the supplier [23].

Material		Carbon mean	Carbon variation
AISI	H13	0.385%	0.32%–0.45%
	P20	0.400%	0.35%–0.45%
	S1	0.475%	0.40%–0.55%
	O1	0.925%	0.85%–1.00%
	D2	1.500%	1.40%–1.60%
	D6	2.125%	2.00%–2.25%
SAE	1020	0.205%	0.18%–0.23%
	1045	0.465%	0.43%–0.50%
	5160	0.600%	0.56%–0.64%

2.3. Image processing and feature extraction

All the images from the ensemble were converted into grayscale. The grayscale is computed from the information of RGB (Red, Green and Blue) color space and contains valuable information on the color differences between materials. The spark test grayscale images shows different textures from different materials. Image textures are commonly analyzed with the histogram information and an interesting measure of the texture characteristic using the histogram information is the entropy. The entropy value is also used to measure the organization level of an image [24]. The entropy of an image is given by Eq. (1), where $P(k)$ is the histogram probability mass function of the grayscale image. The entropy was the first feature.

$$E = -\sum_{n=0}^{N-1} P(n) log_2(P(n)). \quad (1)$$

The images were then processed to identify the edges of all the sparks. We used the Canny method [25] to determine those edges. The spark edges information allowed finding the contour of each one. Fig. 5 shows an example of this image processing. By the contour information, the area in pixels of each spark is determined. At this point, all the images with no sparks were discarded.

To analyze the shape of sparks, we studied the distribution of sparks areas in pixels using the box plot graphics presented in Fig. 6. All spark areas greater than the superior limit were discarded. Doing so we eliminated the outliers from larger areas, for example, any larger spark occlusion. As shown in Fig. 4, some materials do not clearly present the flame. Therefore, to equally analyze the sparks shapes in all materials, the larger flame areas were also considered as outliers.

The shape of sparks varies among the different materials and, as consequence its area also varies. The longer the spark, the greater the area. However, not all sparks from the same steel have a constant length or shape, for example, the spark explosion produces tiny areas close to greater areas. This behavior of sparks is presented in 6, noting that all materials have very close inferior limits, indicating the spark explosions and tiny areas, however the superior limit has different values. Also, the range from the first to the third quartile are very different, indicating the variety of sparks shapes in steels, except for D2 and D6, and also for 1045 and 5160. As the second feature, we considered the interquartile range of the box plot. The third feature was the median (second quartile of the box plot).

The quantity of sparks indicates differences among steel samples, for example, the steel D6 in Fig. 4(f) has fewer sparks than P20 in Fig. 4(b). Therefore, the fourth feature was the quantity of sparks. The quantity of sparks and its area represents how the image is filled with its information. For example, the area occupied by sparks of H13 in Fig. 4(a) is greater than S1 in Fig. 4(c). Thus, the sum of all sparks areas was the last feature considered.

(a) H13

(b) P20

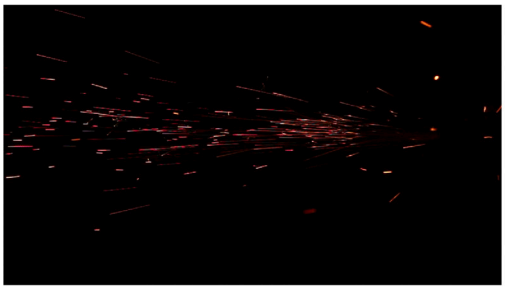

(c) S1

(d) O1

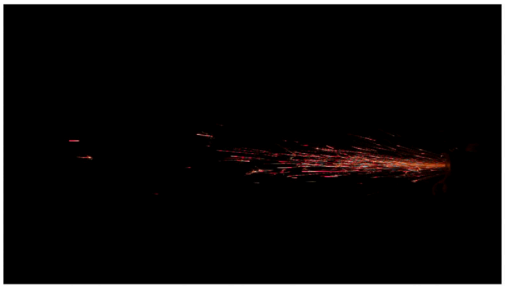

(e) D2

(f) D6

(g) 1020

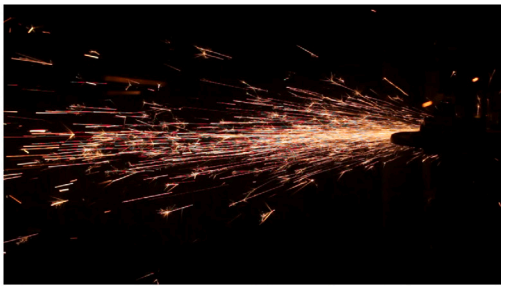

(h) 1045

(i) 5160

Fig. 4. Examples of spark test images from each material.

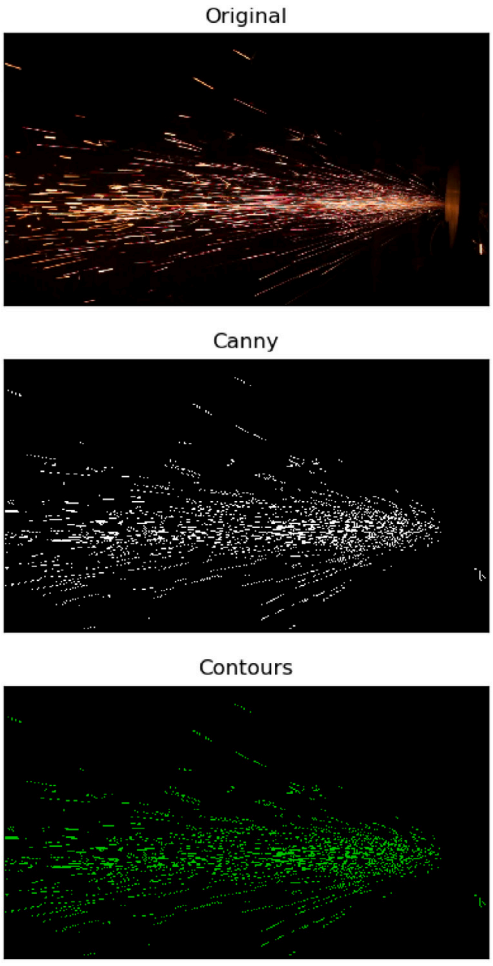

Fig. 5. Example of the sparks image processing. Above is the original image. The Canny segmentation method output is in the middle. Below, in green the contours found by the method implemented in OpenCV.

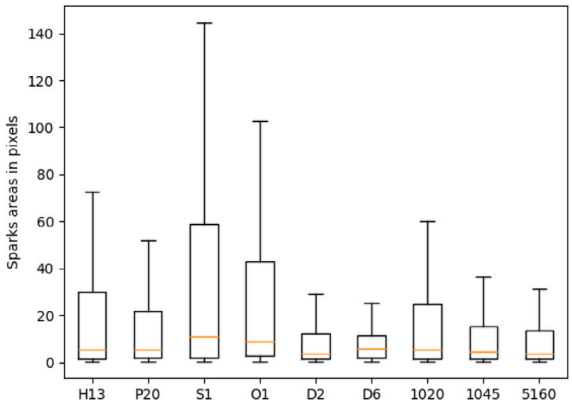

Fig. 6. Analysis of sparks areas in pixels from each material.

2.4. Standardization

The features extracted from the spark test images may vary substantially in scale between each other. For example, the scale difference between the total sparks areas and quantity of sparks. This may introduce errors in algorithm training because machine learning models consider higher values as more important and, consequently, assign higher weights to them. This could reduce the impact of features with smaller scales in the prediction of carbon content or in the classification of steels. Therefore, standardizing the data is extremely important for the good accuracy of the models. We used Eq. (2) to standardize our data.

$$x_{std} = \frac{x - \mu}{\sigma}. \tag{2}$$

Where μ represents the mean and σ the standard deviation of the dataset. This equation computes a new scale to all features in the dataset, with mean equal to zero and a standard deviation of one. This standardization method is also known as Z-score. After standardization, we separated 70% of the dataset for training and 30% for testing the machine learning models.

2.5. Machine learning

In order to identify the steel material we used two different approaches of machine learning models. The first approach aims at estimating the carbon content of steel based on the features extracted from the spark images. Two models performed better in this task, Support Vector Regression (SVR) and Random Forest Regression (RFR). The second approach aims at classifying the steel among our set of materials. After several tests, two models showed good results, the Support Vector Machine (SVM) and K-Nearest Neighbors (KNN).

The SVM is an algorithm that attempts to suit a line (or plan, or hyperplane) between the different classes (in our method, the steel) maximizing the distance of the lines to the points (features) of each class. Therefore, the algorithm seeks for a robust separation between classes [26,27]. The main parameter is the kernel function, in our case the best result was achieved with the Radial Basis Function.

The KNN algorithm makes the classification based on the distance to K points of the training set. This algorithm does not need additional parameters but the K value [28,29]. In this work the best results were achieved with $K = 9$.

The Random Forest Regression is based on classifying decision trees that try to fit a number based on sub-samples of the input dataset. Further, it averages the output to improve the accuracy [30]. In this work, we also used the SVR to estimate the carbon content of each sample. The SVR works similarly to SVM, but the result is a regression based on the input data of the model. We used the features extracted from the images as the input dataset to the four machine learning models.

2.6. Evaluation metrics

The metric used to evaluate the regression models (SVR and RFR) was the mean error. For the classifier models (SVM and KNN) we used the confusion matrix.

The confusion matrix contains the information of true positives (TP), true negatives (TN), false positives (FP) and false negatives (FN) of the classification model. This is the most popular tool to evaluate the classification models. For example, it is desirable that in a perfect classifier all data is deposited diagonally across the matrix. Also, the spariality is related to confounding factors. From the confusion matrix, it is possible to evaluate the model using numerical metrics, we used the accuracy, precision, recall and F1-Score.

The accuracy is described by Eq. (3) and indicates the overall performance of the model. Among all classifications, how many outputs the model classified correctly.

$$accuracy = \frac{TP + TN}{TP + TN + FP + FN}. \tag{3}$$

The recall is given by Eq. (4) and indicates the proportion of positives that were correctly identified. Also known as the true positive rate. If the machine learning model produces no false negatives, the recall is 1.0.

$$recall = \frac{TP}{TP + FN}. \tag{4}$$

Table 2
Number of images per material used on machine learning algorithms.

Material	Total	Train	Test
H13	1060	737	323
P20	1026	707	319
S1	988	714	274
O1	949	654	295
D2	917	667	250
D6	332	238	94
1020	865	585	280
1045	1065	722	343
5160	995	713	282

Table 3
Carbon contents mean error of each steel sample using Random Forest Regression (RFR) and Support Vector Regression (SVR).

Carbon		RFR error	SVR error
Mean	Variation	Mean	Mean
0.205%	0.18%–0.23%	8.4%	9.7%
0.385%	0.32%–0.45%	4.5%	8.8%
0.400%	0.35%–0.45%	4.8%	8.3%
0.465%	0.43%–0.50%	5.6%	7.7%
0.475%	0.40%–0.55%	10.8%	14.7%
0.600%	0.56%–0.64%	4.6%	5.4%
0.925%	0.85%–1.00%	14.5%	16.9%
1.500%	1.40%–1.60%	10.6%	12.6%
2.125%	2.00%–2.25%	15.7%	22.8%

The precision computes among all the positive class classifications the predictions that are actually correct. It is given by Eq. (5). If the machine learning model produces no false positives, the precision is 1.0.

$$precision = \frac{TP}{TP + FP}. \tag{5}$$

The F1Score is the harmonic mean of precision and recall, described by Eq. (6).

$$F1score = 2\frac{precision.recall}{precision + recall}. \tag{6}$$

F1Score is a good measure to evaluate the balance between recall and precision. The closer this score is to 1, the fewer points of confusion in the model.

3. Results

Since the spark method is a destructive test, each of the 9 samples material were divided into 10 parts resulting in 90 samples. We recorded one video for each sample resulting in 8197 images with spark information. From the total of images, 5737 (70%) were used for training and 2460 (30%) for testing the machine learning models. For more details of this division refer to Table 2. The same set of images was used in the four models. We considered nine classes for classification which is the number of materials.

The SVR model has a total error of 10% in estimating the carbon content, while the RFR error was 8%. Thus, the RFR had a slightly better result than the SVR. We also investigated the results of the regression models in estimating the carbon content individually. The Table 3 shows the mean error for each estimate. Again, the RFR model presented better results than SVR for all materials. Focusing on the RFR model, note that the mean error, in general, has low values. The RFR model had the lower mean error of 4.5% at 0.385% and the higher mean error of 15.7% at 2.125% of carbon.

The carbon values of 0.385%, 0.400%, 0.465% and 0.475% are very close to each other and also have an overlap in the variations. However, the RFR model estimated the carbon value with a low error even in steel samples with close percentage values. Of course, the overlap of variations may cause confusion if this is the only analysis model.

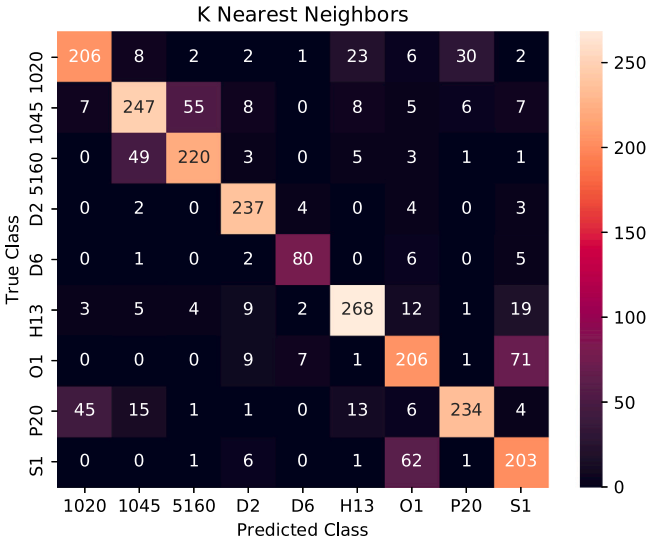

Fig. 7. KNN confusion matrix.

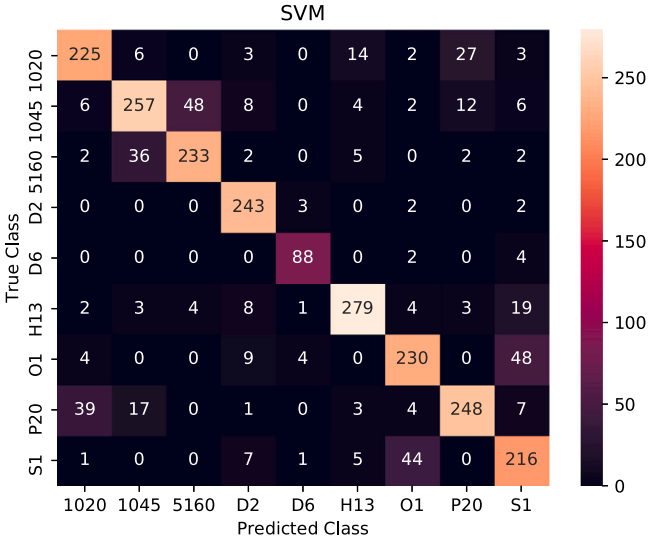

Fig. 8. SVM confusion matrix.

However, even an experienced operator may have the same confusion, therefore this behavior indicates a coherence of the model with the manual spark test.

To decrease the confusion at overlaps intervals, we also implemented the classification models for the same set of images. For this task, the KNN and SVM models were used. The KNN model has an accuracy of 77%, the results are presented by a confusion matrix in Fig. 7. The confusion matrix of SVM model is presented in Fig. 8. The SVM model has an accuracy of 82%. Note that the KNN and SVM confusion matrices are consistent in terms of their spariality. There is also consistency in the most confusing points. Both classification models had good results and the classes that the models committed greater mistakes are the same: 1020 with P20, 1045 with 5160, and S1 with O1.

From the confusion matrix we computed the evaluation metrics and the results are presented in Table 4. From these scores it is clear that SVM model showed better results in classifying steel. The precision with greater scores was for D2, D6 and H13. This indication represents a low number of false positives. D2 and D6 had higher scores on recall which indicates a low number of false negatives. The worst scores were for S1, presenting the higher number of false positives and false negatives.

Table 4
Evaluation metrics of KNN and SVM.

Material	Precision		Recall		F1score	
	SVM	KNN	SVM	KNN	SVM	KNN
1020	81%	79%	80%	74%	81%	76%
1045	81%	76%	75%	72%	78%	74%
5160	82%	78%	83%	78%	82%	78%
D2	86%	86%	97%	95%	92%	90%
D6	91%	85%	94%	85%	92%	85%
H13	90%	84%	86%	83%	88%	83%
O1	79%	66%	78%	70%	79%	68%
P20	85%	85%	78%	73%	81%	79%
S1	70%	64%	79%	74%	74%	69%

In the SVM confusion matrix shown in Fig. 8, it is desirable that most classifications appear on the main diagonal of the matrix. However, three mistakes are clearly presented, the misclassification of 1020 with P20, 1045 with 5160, and S1 with O1. The errors are caused because the samples have close visual spark characteristics as examples presented in Fig. 4. This effect occurs due to the fact that steel has other chemical compositions in addition to carbon which biases the sparks' behavior. For example, both S1 and O1 have manganese, chromium, tungsten and carbon. Also, 1045 and 5160 are both carbon steels. The P20 and 1020 confusion is the most intriguing confusion. The P20 is a steel tool with high production variability and that can explain the confusion with 1020. The similarity of the sparks characteristics are also presented in Fig. 6. Note that 1020 has the median close to P20 and the median of S1 and O1 are very close too. The sparks areas distributions of 1045 and 5160 are very similar which contributes to the misclassifications.

Back in Table 1, the steel 1020 has 0.205% and P20 has 0.400% of carbon, thus, using the RFR and SVM together the points with problems in classification can be easily solved because RFR could estimate with a low error the carbon of each sample. The same analysis is suitable to 1045 and 5160, where the carbon values are 0.465% and 0.600% respectively. Also, S1 and O1 have 0.475% and 0.925% carbon values and can be easily distinguished.

In a general way, the classification models had a good separation between steel classes. Again, in Figs. 7 and 8, it is easy to observe that the greater values are in the main diagonal of the confusion matrix. Also, the great number of zero false positives and false negatives shows that the model had a good behavior for steel classification. The D6 and D2 samples are good examples of it. Despite a few problems on steel classifications using SVM, when the analysis was made together with the RFR model it was clear the difference between materials.

4. Conclusions

We proposed a method for classifying and estimate carbon on steel materials using machine learning and image processing in spark test images. We developed a device for fixing the sample and the grinding machine to guarantee the same setup for each video captured from the spark tests. All the frames of the video were then converted into grayscale images. We proposed a set of features extracted from the spark method images that together have a good agreement to carbon content of steel materials. Furthermore, we understand that the proposed method is suitable for real-time applications and feasible on the shop floor.

We discussed two approaches of machine learning models: regression and classifying models. The Random Forest Regression (RFR) model has the better accuracy in carbon estimation of the steel samples. The Support Vector Machine (SVM) classified the steel samples with less error than the K-Nearest Neighbor model (KNN). Both approaches must be used together in order to reduce the misclassifications of the SVM model and improve the accuracy in steel classifications. The classification models had good results on steel classification and in the classes where the SVM showed some mistakes on classification, the carbon value of the steel material was very different. Thus, the RFR could predict the carbon content with low error and help on SVM classification confusion points. Naturally, if the confusion points are in the same carbon content variation interval, the RFR will not help to increase the accuracy for steel determination.

The features proposed have the advantages of being simple and easy to extract from the images. These features together had a good agreement with the carbon content and are suitable for steel classifications. However, other features should be tested in spark method images for better accuracy of the models. One example of it is the opening angle formed by the sparks when detached from the grinder. An accurate detection of explosion sparks should be developed as well. Furthermore, thermal cameras could also reveal different features in images towards a better accuracy in carbon determination or classifying steel.

We tested our method with 9 different steel materials. It would be interesting to extend this work and increase the number of materials. The analysis of the behavior of our method showed robustness in the estimates of carbon concentrations and steel determination. Therefore, we expect the method to have good accuracy for a larger number of materials if the classification and regression models are analyzed together.

CRediT authorship contribution statement

Pedro José Pacheco Kerscher: Conceptualization, Validation, Data Curation, Investigation. **Jean Schmith:** Conceptualization, Methodology, Software, Validation, Data Curation, Investigation, Writing – original Draft, Supervision. **Eduardo Augusto Martins:** Formal analysis, Writing – review & editing. **Rodrigo Marques de Figueiredo:** Formal analysis, Writing – review & editing. **Armando Leopoldo Keller:** Formal analysis, Writing – review & editing.

Declaration of competing interest

The authors declare that they have no known competing financial interests or personal relationships that could have appeared to influence the work reported in this paper.

Acknowledgment

The authors acknowledges Favorit Aços Especiais for providing the steel materials.

References

[1] J.F. Magallanes, C. Vazquez, Automatic classification of steels by processing energy-dispersive X-ray spectra with artificial neural networks, J. Chem. Inf. Comput. Sci. 38 (4) (1998) 605–609.
[2] F. Mohamad, T.S. Cevat, A. Mehdi, P. Farzad, Fracture characteristics of AISI D2 tool steel at different tempering temperatures using acoustic emission and fuzzy c-means clustering, Arab. J. Sci. Eng. 38 (8) (2013) 2205–2217.
[3] J. Dobrzański, M. Sroka, A. Zieliński, Methodology of classification of internal damage the steels during creep service, J. Achiev. Mater. Manuf. Eng. 18 (1–2) (2006).
[4] T. Segreto, A. Simeone, R. Teti, Chip form classification in carbon steel turning through cutting force measurement and principal component analysis, Procedia Cirp 2 (2012) 49–54.
[5] L. Dobrzański, W. Sitek, Application of a neural network in modelling of hardenability of constructional steels, J. Mater Process. Technol. 78 (1–3) (1998) 59–66.
[6] G. Thewlis, Classification and quantification of microstructures in steels, Mater. Sci. Technol. 20 (2) (2004) 143–160.
[7] S.M. Azimi, D. Britz, M. Engstler, M. Fritz, F. Mücklich, Advanced steel microstructural classification by deep learning methods, Sci. Rep. 8 (1) (2018) 1–14.
[8] K. Xu, Y.-h. Ai, X.-y. Wu, Application of multi-scale feature extraction to surface defect classification of hot-rolled steels, Int. J. Minerals Metallurgy Mater. 20 (1) (2013) 37–41.

[9] J. Masci, U. Meier, D. Ciresan, J. Schmidhuber, G. Fricout, Steel defect classification with max-pooling convolutional neural networks, in: The 2012 International Joint Conference on Neural Networks, IJCNN, IEEE, 2012, pp. 1–6.
[10] S. Zhou, Y. Chen, D. Zhang, J. Xie, Y. Zhou, Classification of surface defects on steel sheet using convolutional neural networks, Mater. Technol. 51 (1) (2017) 123–131.
[11] G. Fu, P. Sun, W. Zhu, J. Yang, Y. Cao, M.Y. Yang, Y. Cao, A deep-learning-based approach for fast and robust steel surface defects classification, Opt. Lasers Eng. 121 (2019) 397–405.
[12] I. Konovalenko, P. Maruschak, J. Brezinová, J. Viňáš, J. Brezina, Steel surface defect classification using deep residual neural network, Metals 10 (6) (2020) 846.
[13] A. Caggiano, J. Zhang, V. Alfieri, F. Caiazzo, R. Gao, R. Teti, Machine learning-based image processing for on-line defect recognition in additive manufacturing, CIRP Ann. 68 (1) (2019) 451–454.
[14] L. Liang, T. Zhang, K. Wang, H. Tang, X. Yang, X. Zhu, Y. Duan, H. Li, Classification of steel materials by laser-induced breakdown spectroscopy coupled with support vector machines, Appl. Opt. 53 (4) (2014) 544–552.
[15] T. Zhang, D. Xia, H. Tang, X. Yang, H. Li, Classification of steel samples by laser-induced breakdown spectroscopy and random forest, Chemometr. Intell. Lab. Syst. 157 (2016) 196–201.
[16] A. Beskopylny, A. Lyapin, H. Anysz, B. Meskhi, A. Veremeenko, A. Mozgovoy, Artificial neural networks in classification of steel grades based on non-destructive tests, Materials 13 (11) (2020) 2445.
[17] R. Buzzard, The utility of the spark test as applied to commercial steels, Bur. Stand. J. Res. (1933) 527–540.
[18] T. Dalke, J. Brink, M. Weller, Material determination using spark observation, Global J. Eng. Educ. 15 (3) (2013).
[19] T. Nakata, Development of automated spark testing technique by image processing to measure carbon content in steel materials, IFAC Proc. Vol. 45 (23) (2012) 118–119.
[20] K. Deng, D. Pan, X. Li, F. Yin, Spark testing to measure carbon content in carbon steels based on fractal box counting, Measurement 133 (2019) 77–80.
[21] G. Bradski, The OpenCV Library, Dr. Dobb's J. Softw. Tools (2000).
[22] F. Pedregosa, G. Varoquaux, A. Gramfort, V. Michel, B. Thirion, O. Grisel, M. Blondel, P. Prettenhofer, R. Weiss, V. Dubourg, J. Vanderplas, A. Passos, D. Cournapeau, M. Brucher, M. Perrot, E. Duchesnay, Scikit-learn: Machine learning in python, J. Mach. Learn. Res. 12 (2011) 2825–2830.
[23] A.E. Favorit, Favorit special steel supplier, 2021, URL https://favorit.com.br/.
[24] T. Celik, T. Tjahjadi, Automatic image equalization and contrast enhancement using Gaussian mixture modeling, IEEE Trans. Image Process. 21 (1) (2011) 145–156.
[25] J. Canny, A computational approach to edge detection, IEEE Trans. Pattern Anal. Mach. Intell. (6) (1986) 679–698.
[26] H.M. Nguyen, B. Demir, M. Dalponte, Weighted support vector machines for tree species classification using lidar data, in: IGARSS 2019-2019 IEEE International Geoscience and Remote Sensing Symposium, IEEE, 2019, pp. 6740–6743.
[27] A. Sarkar, M. Maniruzzaman, M.S. Ahsan, M. Ahmad, M.I. Kadir, S.T. Islam, Identification and classification of brain tumor from MRI with feature extraction by support vector machine, in: 2020 International Conference for Emerging Technology, INCET, IEEE, 2020, pp. 1–4.
[28] M. Vaishnnave, K.S. Devi, P. Srinivasan, G.A.P. Jothi, Detection and classification of groundnut leaf diseases using knn classifier, in: 2019 IEEE International Conference on System, Computation, Automation and Networking, ICSCAN, IEEE, 2019, pp. 1–5.
[29] Z. Yu, Research on remote sensing image terrain classification algorithm based on improved KNN, in: 2020 IEEE 3rd International Conference on Information Systems and Computer Aided Education, ICISCAE, IEEE, 2020, pp. 569–573.
[30] D. Jayaraj, S. Sathiamoorthy, Random forest based classification model for lung cancer prediction on computer tomography images, in: 2019 International Conference on Smart Systems and Inventive Technology, ICSSIT, IEEE, 2019, pp. 100–104.